Available online at www.sciencedirect.com
SCIENCE DIRECT®
Catalysis Today 90 (2004) 3–14
CATALYSIS TODAY
www.elsevier.com/locate/cattod

Ammonia oxidation over $Au/MO_x/\gamma\text{-}Al_2O_3$—activity, selectivity and FTIR measurements

Shawn D. Lin [a], Andreea C. Gluhoi [b], Bernard E. Nieuwenhuys [b,*]

[a] *Department of Chemical Engineering, Yuan Ze University, Taiwan, Taiwan ROC*
[b] *Department of Heterogeneous Catalysis and Surface Chemistry, Leiden Institute of Chemistry, Leiden University, P.O. Box 9502, 2300 RA Leiden, The Netherlands*

Available online 15 June 2004

Abstract

The selective catalytic oxidation (SCO) of NH_3 was studied over various $\gamma\text{-}Al_2O_3$-supported gold-based catalysts at 2% NH_3 + 2% O_2 (balance He). The effects of different kinds of oxidic additives, MO_x (M = Cu, Fe, Ce, Li, and Ti) were examined. The mixed metal oxides, MO_x–Al_2O_3, were used as supports of 5% Au catalysts. The presence of Au enhances the SCO activity. The following order of per-gram activity was found in the temperature range from 473 to 673 K: $Au/Ti\text{-}Al_2O_3 < Au/Al_2O_3 \approx Au/TiO_2 < Au/Li\text{-}Al_2O_3 < Au/FeO_x \approx Au/Fe\text{-}Al_2O_3 < Cu\text{-}Al_2O_3 \approx Au/Ce\text{-}Al_2O_3 < Au/Li–Ce\text{-}Al_2O_3 \leq Au/Cu\text{-}Al_2O_3$. The selectivity is strongly dependent on the type of MO_x used. The most active catalyst $Au/Cu–Al_2O_3$ shows a conversion of 50% at 483 K and a N_2 selectivity over 90%. On the other hand, $Au/Li–Ce\text{-}Al_2O_3$, which has an only slightly lower activity than $Au/Cu/Al_2O_3$ is very selective to N_2O. FTIR spectroscopy shows bands following NH_3 adsorption that can be attributed to imide-like (–NH) adspecies, in addition to NH_4^+ (on Brønsted acid sites) and coordinated NH_3 (on Lewis acid sites). The presence of Au enhances the band intensity of imide-like adspecies, which may be responsible for the improved SCO activity in the presence of Au.

Keywords: Gold; Ammonia; Oxidation; Oxides; Selectivity; FTIR

1. Introduction

Ammonia is a commonly used reducing agent in the selective catalytic reduction (SCR) of NO_x. However, the emission of unreacted ammonia becomes a secondary air pollution problem because ammonia itself is hazardous. Therefore, selective catalytic oxidation (SCO) is needed to convert traces of NH_3 at the downstream of the SCR reactor to N_2 via reaction (1)

$$4NH_3 + 3O_2 \rightarrow 2N_2 + 6H_2O \quad (1)$$

$$4NH_3 + 4O_2 \rightarrow 2N_2O + 6H_2O \quad (2)$$

$$4NH_3 + 5O_2 \rightarrow 4NO + 6H_2O \quad (3)$$

Such a SCO reaction may also be used for the control of other ammonia emission sources, e.g. agricultural sources and nitric acid production plants. There are two important issues about this SCO reaction: one is the selectivity and the other is the application temperature. The oxidation of ammonia can also produce NO_x via reactions (2) and (3) which makes the selectivity of SCO reaction critical. Potentially, N_2O may be used for SCO of hydrocarbons [1,2]. Therefore, it would be interesting to develop a catalyst with a high selectivity to N_2O (Reaction (2)). Operation at high-temperatures (>800 K) selectively produces NO and this Ostwald process is used for many years for the industrial production of nitric acid [3]. Noble-metal catalysts (Pt with Rh) are used for this purpose. Therefore, a lower SCO reaction temperature should be better for NH_3 abatement. In addition, if the SCO were to be used at the downstream of a SCR unit, an application temperature lower than 573 K would be desired. Unsupported [4] and supported oxide catalysts [5–9] were found to give quite a good N_2 selectivity but their activities are not sufficient at temperatures below 573 K. Noble metal catalysts were reported to be more active in this temperature range, but less selective to N_2 than oxide catalysts [10,11]. Amblard et al. [12,13] reported that

* Corresponding author. Tel.: +31 71 527 4545; fax: +31 71 527 4451.
E-mail addresses: sdlin@saturn.yzu.edu.tw (S.D. Lin), b.nieuwe@chem.leidenuniv.nl (B.E. Nieuwenhuys).

0920-5861/$ – see front matter © 2004 Elsevier B.V. All rights reserved.
doi:10.1016/j.cattod.2004.04.047

Ni/Al_2O_3 could be a good SCO catalyst. Long and Yang recently reported a better SCO performance for Fe-ZSM5 compared to other metal-exchanged ZSM-5 catalysts [14]. They tried further to improve the performance of Fe-based catalysts by using different types of zeolites [15], different oxide supports [9], and by the addition of a noble metal [11]. On the other hand, Gang et al. [8] found a better SCO performance of Cu–Y compared to other metal-exchanged NaY or Al_2O_3-supported metal oxides. Their studies were later directed toward Al_2O_3-supported Cu [16], Ag [17], and Cu–Ag [18]. The performance of these catalysts will be compared to those of the catalysts used in this study.

Au catalysts are known for their unusually high oxidation activity at low temperatures, especially toward CO [19,20]. However, to the best of our knowledge ammonia oxidation over Au catalysts has not been reported in the literature. The present paper describes a study concerning the SCO of ammonia over gold-based catalysts supported on γ-Al_2O_3 with additives consisting of different kinds of oxides, viz. the oxides of Cu, Fe, Ti, Ce, and Li. Cu was selected because of its high intrinsic activity in NH_3 oxidation with an excellent selectivity to N_2. Ti and Fe were chosen because of the high catalytic activity of multicomponent catalysts consisting of Au and transition metal oxides for certain reactions. For the same reason ceria was used. Alkali metal oxides are used as promoters for a large number of catalytic processes. In addition, it was reported that the addition of Li_2O to Au/Al_2O_3 results in an improved activity for various oxidation reactions [21].

2. Experimental

2.1. Catalyst preparation

Mixed oxides were prepared by impregnating γ-Al_2O_3 (Engelhard Al-4172P, 275 $m^2\,g^{-1}$) with nitrates of Cu, Li, Fe, Ce or with Ti-butoxides. After calcination at 623 K, the mixed oxides were used as supports for Au catalysts and are designated as M-Al_2O_3 hereafter. The prepared mixed oxides typically have an M/Al atomic ratio of 1/15 unless otherwise specified. Au catalysts were prepared via $HAuCl_4{\cdot}3H_2O$ (Aldrich) deposition using urea as the precipitating agent. The filtered powders were thoroughly washed to remove Cl^- residues. All catalysts were calcined at 573 K afterwards. Details of the catalyst preparation have been reported earlier [21]. A 5% Au loading was used for all the Au catalysts. For comparison, Au/TiO_2 and Au/Fe_2O_3 were prepared in a similar way using commercial TiO_2 (Eurotitania 1) and Fe_2O_3 prepared by the precipitation from $Fe(NO_3)_3{\cdot}6H_2O$ (Aldrich).

2.2. Catalyst characterization

The gold loading was verified by atomic absorption spectroscopy (AAS) using a Perkin-Elmer 3100 with an air/acetylene flame [21]. For that purpose, the catalysts were dissolved in aqua regia and the solution was diluted with demineralized water before performing the analysis.

BET surface areas of the catalysts were measured by N_2 physisorption at 77 K using an automatic Qsurf M1 analyzer. Before each measurement the catalyst was heated in helium at 473 K for 2 h in order to remove impurities adsorbed on the surface.

X-ray diffraction measurements were performed using a Philips Goniometer PW 1050/25 diffractometer equipped with a PW Cu 2103/00 X-ray tube operating at 50 kV and 40 mA. The average gold particle size was estimated from XRD line broadening after subtraction of the signal from the corresponding support by using the Scherrer equation.

2.3. Activity measurements

Ammonia oxidation was carried out in a microreactor system using quartz reactors. The feed gases were controlled by mass flow controllers (Bronkhorst) and set to a total flow of 30 ml min^{-1}. NH_3 (4% in He, Hoek Loos) and O_2 (4% in He, Hoek Loos) were used without further treatment to make a feed containing 2% NH_3 and 2% O_2. The catalyst was pretreated in situ with hydrogen up to 573 K, followed by a cool-down under He to 298 K. The test procedures started with feeding 4% O_2 until the gas composition was stabilized, subsequent feeding an equal flow rate of 4% NH_3 until stabilized, thereafter the reactor was ramped through at least two heating-cooling cycles at 5 K/min up to 673 and 623 K, respectively. A mass spectrometer (Balzers, Q422) was used to monitor the effluent composition via a differential pumping interface. The monitored mass signals include 2, 14, 16, 17, 18, 28, 30, 32, 44, and 46. After corrections of the signal intensities for the fragmentation signals of the different compounds, the effluent material balance in the heating sequences was correct within ±10% of the feed, but not in the cooling sequences. The erroneous material balance in the cooling sequences is attributed to the slow pumping of H_2O and NH_3. Therefore, only the data in the heating sequences is used for activity analysis.

FTIR analysis was carried out using a commercial instrument (Mattson, Galaxy 2020) equipped with a controlled-atmosphere chamber. The IR spectrum was measured in the transmission mode at a resolution of 2 cm^{-1} and corrected for the background spectrum, which was averaged from 50 scans of the empty cell (at pressures better than 10^{-3} Pa). A self-supporting wafer was made from catalyst powders. After mounting, the wafer was evacuated to 10^{-1} Pa, then subjected to a heat-treatment to 573 K under 2×10^4 Pa of hydrogen and a following cool-down at which evacuation started at around 500 K. Both M-Al_2O_3 and the supported Au/M-Al_2O_3 catalysts were pretreated in this way. An IR spectrum was recorded at 313 K and 10^{-3} Pa after this treatment and was used as the reference to latter-recorded spectra of the same sample. Thereafter,

2×10^3 Pa of NH_3 was introduced, held for 20 min, and evacuated at 313 K. A stepwise temperature-programmed desorption (sTPD) was performed sequentially at 313, 328, 343, 363, 393, 423, 473, 523, and 573 K under vacuum, where an IR spectrum was taken at every temperature. Afterwards the sample was cooled down to 313 K, exposed to NH_3 and a stepwise temperature-programmed oxidation (sTPO) experiment was carried out, which was essentially a sTPD in the presence of approximately 2×10^3 Pa of oxygen. No useful information could be extracted within the region of the N–H stretching modes, because most spectra were very noisy in that region.

3. Results

3.1. Catalysts characterization

AAS measurements show that the catalyst preparation method resulted in a gold loading close to the target loading of 5 wt.% (see Table 1). In the same table are also mentioned the surface areas of the samples determined by BET. For most of the catalysts these values did not differ significantly from those of the bare supports ($275\ m^2\ g^{-1}$ for γ-Al_2O_3 and $37\ m^2\ g^{-1}$ for Eurotitania).

All the samples showed the X-ray diffraction peaks that correspond to metallic gold. For several catalysts the diffraction lines corresponding to the metal oxide additives were found. However, for some samples the formal oxidation state of these oxides could not be identified unambiguously. In these cases, the metal oxide additives are presumably present as highly dispersed on Al_2O_3. From XRD line broadening the average Au particle size was determined (see Table 1).

Table 1
Characterization of gold-based catalysts

Catalyst	Au loading (wt.%)	S_{BET} ($m^2\ g^{-1}$)	d_{Au}^{XRD} (nm)
Al_2O_3	–	275	–
Au/Al_2O_3	4.7	260	4.3 ± 0.1
$Au/CuO/Al_2O_3$ (Cu:Al = 1:15)	3	–	<3
$Au/CuO/Al_2O_3$ (Cu:Al = 1:10)	4.6	–	<3
$Au/CuO/Al_2O_3$ (Cu:Al = 1:5)	5	212	7 ± 0.2
$Au/CeO_x/Al_2O_3$	4.5	218	<3
$Au/Li_2O/Al_2O_3$	4.0	278	3.3 ± 0.1
$Au/Li_2O/CeO_x/Al_2O_3$	4.6	262	<3
Au/TiO_2	4.9	38	3.9 ± 0.2
$Au/TiO_x/Al_2O_3$	4.7	243	<3
$Au/FeO_x/Al_2O_3$	4	234	3.1 ± 0.2

Since the peak width at half maximum intensity was used to determine the average particle size, smaller crystallites were not taken into consideration.

3.2. SCO over Cu-Al_2O_3 and Au/Cu-Al_2O_3

Fig. 1 shows the variation of the NH_3 conversion with increasing temperature over Au/Cu-Al_2O_3 and Cu-Al_2O_3 catalysts with different Cu/Al loading ratios. The peculiar line shape of the data at lower temperatures (below 423 K) is due to initial NH_3 adsorption at room temperature and subsequent NH_3 desorption from 313 to 423 K. Adsorption results in higher apparent conversions in the beginning of the heating sequence, while NH_3 desorption results in negative conversions. Oxygen consumption was not observed in this temperature range. Cu-Al_2O_3 catalysts show a conversion light-off at approximately 523 K. The variation of the Cu content of Cu/Al from 1/5 to 1/15 in Cu-Al_2O_3 did not result in a significantly different behavior.

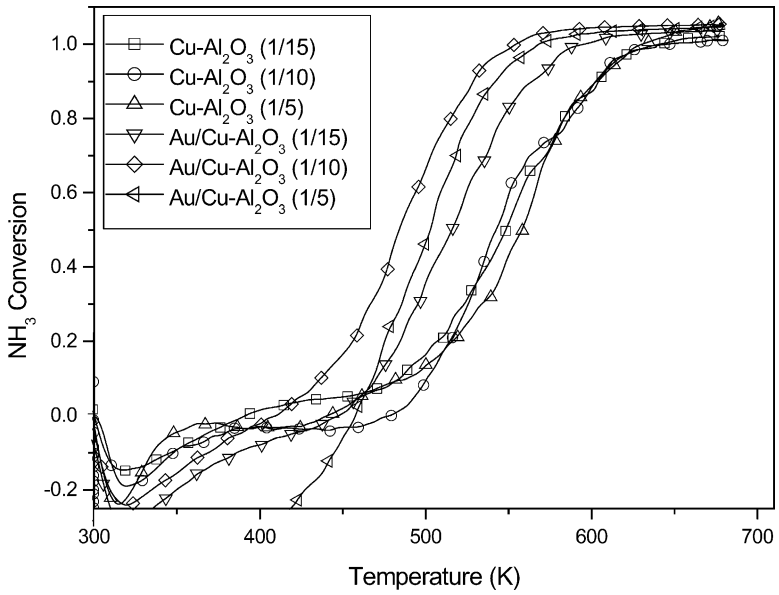

Fig. 1. NH_3 oxidation over Au/Cu-Al_2O_3 and Cu-Al_2O_3 with different Cu loadings. The relevant masses were measured every 5 K but symbols are shown every 20 K.

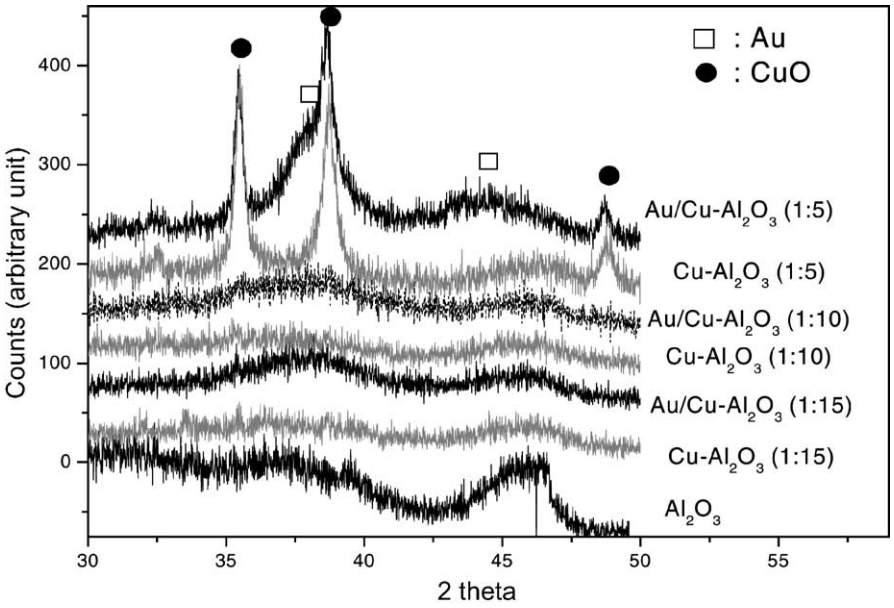

Fig. 2. X-ray diffraction spectra of fresh Cu-Al_2O_3 and Au/Cu-Al_2O_3.

The onset temperature is defined as the temperature corresponding to ≥10% NH_3 conversion. Fig. 1 shows that the onset temperatures over Au/Cu-Al_2O_3 catalysts are 30–50 K lower than over Cu-Al_2O_3. Hence, it can be concluded that the Au/Cu-Al_2O_3 catalysts are clearly more active than Cu-Al_2O_3. This indicates that the presence of Au enhances the activity. Among the three different Cu loadings, a Cu/Al ratio of 1/10 seems to give the best activity for Au/Cu-Al_2O_3. However, the activity recorded in the second heating sequence indicates that a Cu/Al of 5 or 10 showed similar activities though they are both still more active than Au/Cu-Al_2O_3 (Cu/Al = 1/15). This is because that all catalysts except Au/Cu-Al_2O_3 (Cu/Al = 1/5) showed an approximately 5–10% activity decay in the second heating sequence compared to the first heating cycle. The XRD spectra shown in Fig. 2 indicate the presence of CuO-aggregates in the Cu-Al_2O_3 catalyst with Cu/Al = 1/5 and the corresponding Au/Cu-Al_2O_3 catalyst. A rough estimate also indicates that a ratio of Cu/Al = 1/5 is higher than needed for one theoretical monolayer coverage whereas a ratio of Cu/Al = 1/10 is close to a monolayer. The absence of CuO-aggregates in the Cu-Al_2O_3 catalyst with Cu/Al = 1/10 suggests that Cu oxide tends to spread over the Al_2O_3 surface to form well-dispersed CuO. This would imply that at the high Cu loading of Cu/Al = 1/5 both well dispersed CuO and CuO-aggregates are present. That the Au/Cu-Al_2O_3 catalyst with Cu/Al = 1/15 showed a lower activity than the other two Au/Cu-Al_2O_3 catalysts with higher Cu/Al ratio may be due to an incomplete coverage of CuO on Al_2O_3. This may suggest that a well-dispersed CuO surface works as a better substrate for Au than bare Al_2O_3. The presence of a CuO-aggregate in Au/Cu-Al_2O_3 (Cu/Al = 1/5) seems to result in a larger Au particle size than those with lower Cu-loading, as indicated by the Au XRD signals shown in Fig. 2 and Table 1. This may be a reason for the somewhat lower activity of the catalyst with Cu/Al = 1/5 than that with Cu/Al = 1/10.

Gang et al. [18] reported that Cu/Al_2O_3 and Cu-Ag/Al_2O_3 after calcination at 773 K exhibit an excellent activity and N_2 selectivity for SCO reaction. For comparison, the Cu-Al_2O_3 (Cu/Al = 1/10) catalyst was also tested following calcination at 773 K. Fig. 3 compares its activity and selectivity to that pretreated with H_2 at 573 K. It is interesting to note that calcination of this catalyst indeed resulted in an improved activity. It is expected that an O_2 treatment at 773 K results in oxidized Cu which readily catalyzes NH_3 oxidation even at room temperature. However, the better activity was found only in the beginning of the first heating sequence. This is illustrated in Fig. 3, which shows the NH_3 conversion and the selectivity during the first and second heating cycle for calcined and reduced Cu-Al_2O_3 (Cu/Al = 1/10). The oxidized Cu became partly reduced under the reaction conditions used in this study. The N_2 selectivity is over 90%. The effect of the pretreatment on the selectivity is very small.

3.3. SCO over various Au/M-Al_2O_3 catalysts

Fig. 4 compares the ammonia oxidation over all other Au catalysts in the first heating cycles. Au/Fe-Al_2O_3 showed a high initial activity. However, the observed activity of Au/Fe-Al_2O_3 in the second heating sequence is almost the same as that shown for Au/Fe_2O_3. Subsequent heating cycle did not affect the performance of Au/Fe_2O_3. However, Au/Fe-Al_2O_3, just like the calcined Cu-Al_2O_3 catalyst exhibit a slightly higher initial activity in the first heating cycle than in the second and further cycle. Based on the NH_3 conversion in the temperature range from 473 to 673 K, the per-gram activities of all the tested Au catalysts can be

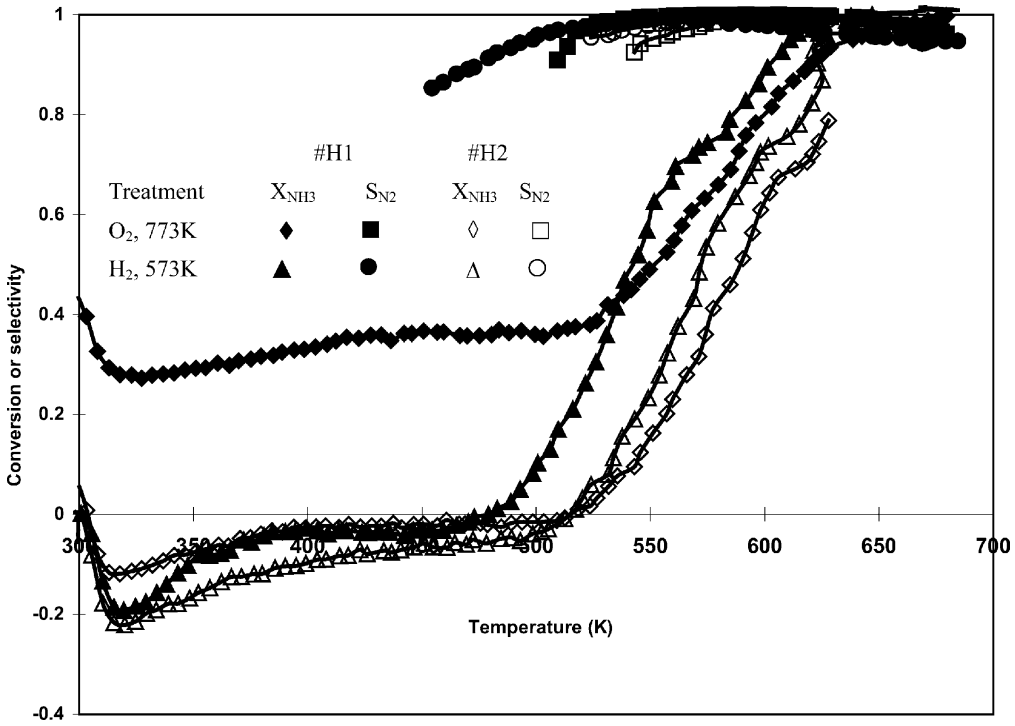

Fig. 3. Effect of pretreatment of Cu-Al_2O_3 (Cu/Al = 1/10) on the NH_3 oxidation during two heating sequences. The conversions during the second heating cycle are somewhat lower than those found in the first heating cycle.

ranked in the following order: Au/Ti-Al_2O_3 < Au/Al_2O_3 ≈ Au/TiO_2 < Au/Li-Al_2O_3 < Au/Fe_2O_3 ≈ Au/Fe-Al_2O_3 < Cu-Al_2O_3 ≈ Au/Ce-Al_2O_3 < Au/Li-Ce-Al_2O_3 ≤ Au/Cu-Al_2O_3. It should be mentioned that the mixed metal oxides (M-Al_2O_3 with M/Al = 1/15) alone were also tested and were found to be negligibly active under identical reaction conditions, except Cu-Al_2O_3 as discussed before. This indicates that the catalytic activity shown in Fig. 4 comes mainly from the presence of Au. XRD analyses (Table 1) of these fresh Au catalysts indicate that the Au particle size sequence show no match to the activity sequence. Hence, the nature of the support plays a decisive role in the differences in SCO activity of the catalysts tested.

The Au/Li–Ce-Al_2O_3 catalyst shows the highest activity of the catalysts shown in Fig. 4. Its activity is rather similar to that of Au/Cu-Al_2O_3 shown in Fig. 1. However, the selectiv-

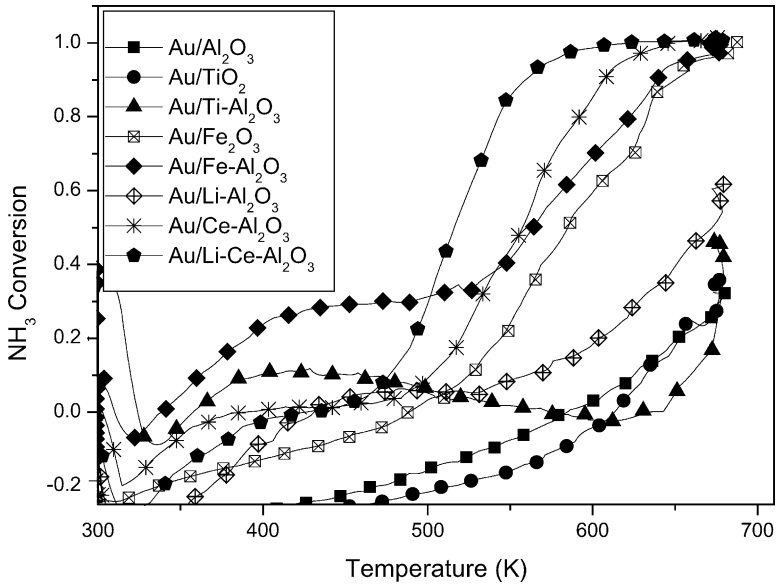

Fig. 4. NH_3 conversion over various Au/M-Al_2O_3 catalysts.

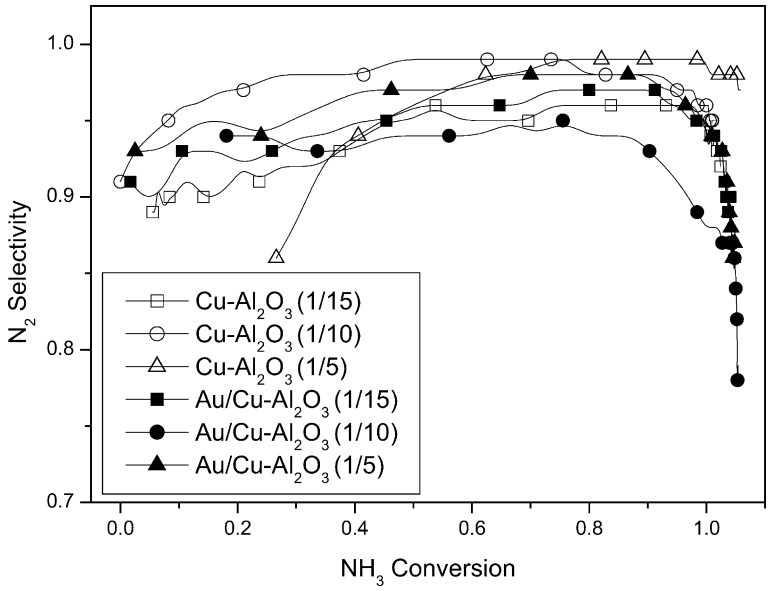

Fig. 5. The N_2 selectivity vs. NH_3 conversion during NH_3 oxidation over Au/Cu-Al_2O_3 and Cu-Al_2O_3 catalysts with different Cu loadings.

ity data shows that Au/Li–Ce-Al_2O_3 produces large amounts of N_2O. Once again, this demonstrates the importance of the support. Fig. 6 depicts the variation of the nitrogen selectivity of these catalysts with increasing NH_3 conversion, in order to ratio the different activities observed in different catalysts. It should be noted that the data shown in Figs. 5 and 6 are adapted from the higher-temperature (>473 K) range in the first heating sequences. This is to avoid the interference from NH_3 adsorption and desorption. It is clear that only Cu-Al_2O_3, Au/Cu-Al_2O_3, and Au/Fe_2O_3 show good N_2 selectivity, whereas Au/Li_2O–CeO_x–Al_2O_3 exhibits a high selectivity to N_2O at temperatures higher than 500 K.

Table 2 summarizes the temperature of 50% conversion (for the first heating stage, #h1, and the second and further heating stages, #h2) as well as the corresponding selectivity to N_2 during #h1. In general, the difference between the first and second (and further) heating cycles does not exceed 20 K. Once again, Au/CuO–Al_2O_3 (Cu/Al = 1/10) performs the best in NH_3 oxidation, in both respects: the NH_3 conversion and the selectivity to N_2. On the other hand, an important synergistic effect is observed for Au/Li_2O–CeO_x–Al_2O_3, with a $T_{50\%}$ of 516 K, compared to $T_{50\%}$ = 553 K for Au/CeO_x–Al_2O_3 and $T_{50\%}$ = 669 K for Au/Li_2O–Al_2O_3.

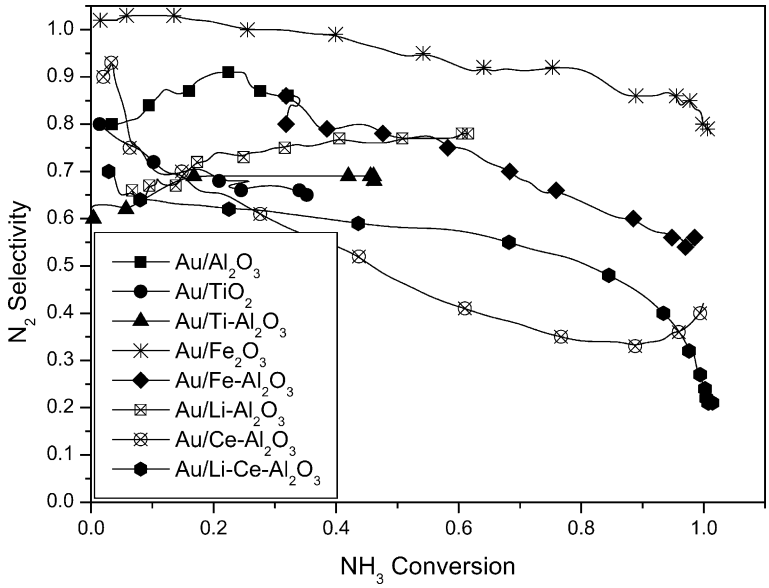

Fig. 6. The N_2 selectivity vs. NH_3 conversion during NH_3 oxidation over various Au/M-Al_2O_3 catalysts.

Table 2
Oxidation of NH_3 over gold-based catalysts: $T_{50\%}$ during the first heating cycle (#h1) and the second heating cycle (#h2), and the corresponding selectivity to N_2 during #h1

Catalyst	$T_{50\%}$ (#h1) (K)	$T_{50\%}$ (#h2) (K)	S_{N_2} (%)
Au/Al_2O_3	>673	>673	–
$Au/CuO/Al_2O_3$ (Cu:Al = 1:15)	518	528	96
$Au/CuO/Al_2O_3$ (Cu:Al = 1:10)	484	503	94
$Au/CuO/Al_2O_3$ (Cu:Al = 1:5)	559	571	96
CuO/Al_2O_3 (Cu:Al = 1:15)	549	589	95
CuO/Al_2O_3 (Cu:Al = 1:10)	536	568	99
CuO/Al_2O_3 (Cu:Al = 1:5)	559	593	96
$Au/CeO_x/Al_2O_3$	553	568	45
$Au/Li_2O/Al_2O_3$	669	>623	77
$Au/Li_2O/CeO_x/Al_2O_3$	516	531	58
Au/TiO_2	>673	>623	–
$Au/TiO_x/Al_2O_3$	>673	>623	–
$Au/FeO_x/Al_2O_3$	564	610	77
Au/Fe_2O_3	585	603	94

3.4. FTIR of NH_3 adsorbed over M-Al_2O_3 catalysts

On oxide surface ammonia can adsorb on both Brønsted and Lewis acid sites. Infrared absorption of NH_4^+ adspecies (on Brønsted acid sites) are found at 1450–1480 and 1660–1690 cm^{-1} for the asymmetric and symmetric deformation modes, respectively. The bands reported for coordinated NH_3 adspecies (on Lewis acid sites) are at 1250–1300 and 1600–1630 cm^{-1}, respectively [22]. Fig. 7 shows the FTIR spectra of NH_3 adsorption on several M-Al_2O_3 at 313 K. It is clear that most of the NH_3 absorption bands can be attributed to these adsorption modes. This indicates that NH_3 adsorbs mainly through Brønsted and Lewis sites. However, these bands have different intensity ratios on the various M-Al_2O_3 catalysts. By comparing the intensity ratios of δ_{sym,NH_3} (approximately 1620 cm^{-1}) to δ_{sym,NH_4^+} (approximately 1690 cm^{-1}), it can be concluded that the fraction of Lewis acid sites increases according to: Li-Al_2O_3 < Ce-Al_2O_3 < Ti-Al_2O_3 < Fe-Al_2O_3 < Al_2O_3 < Cu-Al_2O_3. The observation that Cu-Al_2O_3 shows no Brønsted acid sites is consistent with earlier reports [23–25]. Clearly, the order in concentration of the Lewis-sites does not match the trend of increasing ammonia oxidation activity shown in Figs. 1 and 4. This suggests that the Lewis acid site density on oxide surfaces cannot account for all the differences in the catalytic activities.

A closer examination of the spectra shown in Fig. 7 indicates that the spectra are more complicated and, hence, that an explanation in terms of just NH_4^+ and coordinated NH_3 adspecies is too simple. Both the broad bands at 1150–1300 and 1450–1550 cm^{-1} seem to contain more than one absorption band. For example, Li-Al_2O_3 exhibits a broad band at 1150–1300 cm^{-1} that can be identified as a more intense peak at 1232 cm^{-1} with two shoulders at 1192 and 1263 cm^{-1}. The same band on Fe-Al_2O_3 appears to be a combination of the 1192 and 1232 cm^{-1} bands where the 1192 cm^{-1} peak is more intense. By considering that all the M-Al_2O_3 were subjected to a H_2 treatment at 573 K before IR analysis, the observed 1232 and 1192 cm^{-1} bands are consistent with coordinated NH_3 on oxidized and reduced Fe_2O_3 at 1220 and 1190 cm^{-1}, respectively, as reported in

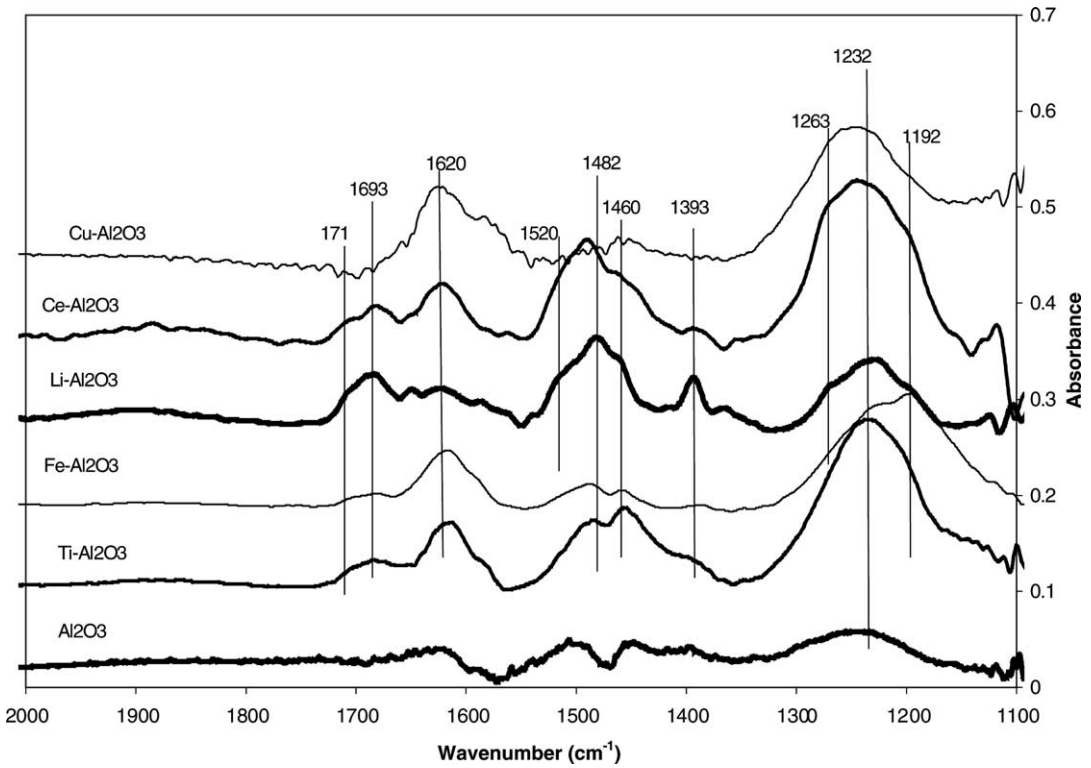

Fig. 7. FTIR spectra of NH_3 adsorption on different M-Al_2O_3 catalysts at 313 K.

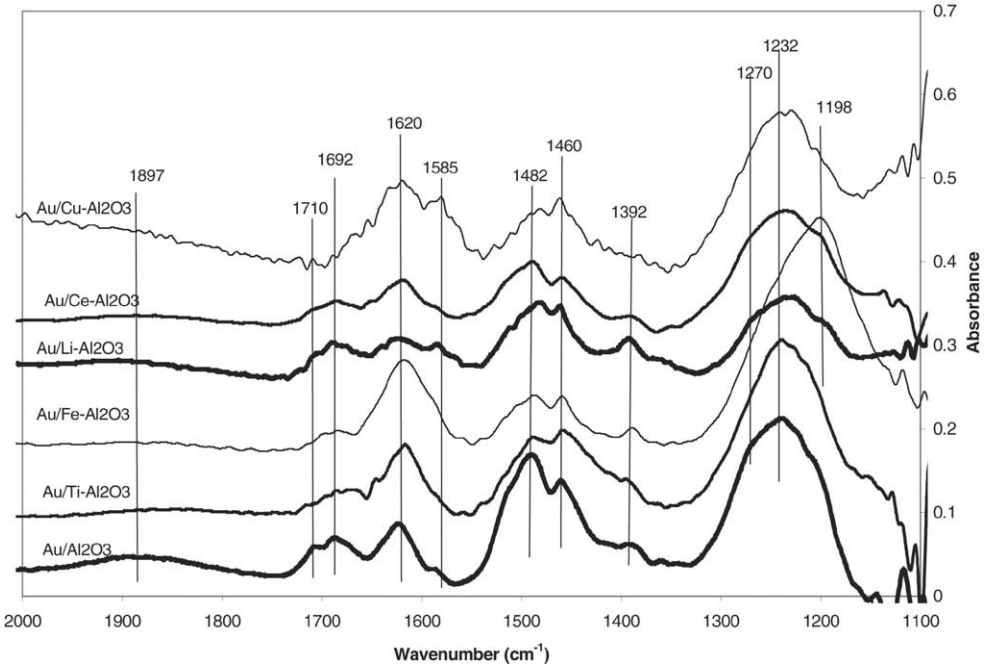

Fig. 8. FTIR spectra of NH_3 adsorption on different Au/M-Al_2O_3 catalysts at 313 K.

[22]. It indicates that Fe-Al_2O_3 may be partially reduced following the pretreatment used in this study. The presence of oxidic Fe in Au/Fe-Al_2O_3 was considered to be responsible for the initial activity enhancement as mentioned earlier. However, in case of Li-Al_2O_3 it is clear that the broad band at around 1230 cm^{-1} cannot be attributed to a partially reduced surface. Alternatively, the multiple-band absorption in this range can be assigned to the presence of different kinds of Lewis acid sites [22,24–30]. However, the situation may be more complicated as will be discussed later.

3.5. FTIR of NH_3 adsorbed over Au/M-Al_2O_3 catalysts

Fig. 8 shows the FTIR spectra of adsorbed NH_3 at 313 K on the different supported Au catalysts used in this study. Gold-based catalysts exhibit absorption bands at 1232, 1392, 1460, 1482, 1585, 1620, 1692, and 1897 cm^{-1}. The bands at 1393, 1482, and 1692 cm^{-1} are close to the bands attributed to the deformation modes of NH_4^+ on γ-Al_2O_3 at 1393, 1478, and 1686 cm^{-1} [30] and are consistent with earlier reports [22,31]. The 1232 and 1620 cm^{-1} bands in Fig. 8 could be assigned to NH_3 adspecies on γ-Al_2O_3 [22,30,31]. On the other hand, the 1232 cm^{-1} band and its shoulder peaks could have another origin. It was reported that amide-like (–NH_2) adspecies (or hydrazine) might be present following NH_3 adsorption on different oxides [22,31–33] and mixed oxides [22–29]. Peri [31] assigned a 1510 cm^{-1} band to the –NH_2 bending mode on Al_2O_3. Bands at 1187, 1210, 1560, and 1610 cm^{-1} were assigned to the NH_2 rocking, ν_{N-N}, δ_{asy,NH_2} and δ_{sym,NH_2} modes of hydrazine on Cu/TiO_2 [27]. The presence of hydrazine may explain the 1192, 1232, and 1585 cm^{-1} bands in Fig. 8. The presumed 1610 cm^{-1} peak of surface hydrazine may overlap with the symmetric deformation mode of coordinated-NH_3 at around 1620 cm^{-1}.

Following the band assignments of NH_4^+, coordinated-NH_3, and amide (or hydrazine) adspecies on Au/M-Al_2O_3, this still leaves the 1460 and the broad 1897 cm^{-1} bands in Fig. 8 unassigned. Kagami et al. [32] attributed a 1410 cm^{-1} band to the imido (–NH) species following NH_3 adsorption on MgO. Bi-dentate NH surface species at 1480 cm^{-1} were reported on CuO/TiO_2 [29] and at 1440–1450 cm^{-1} on MO_x/TiO_2 [28]. This is close to the 1460 cm^{-1} band in Fig. 8 and, therefore, this band is tentatively assigned to an imide-like adspecies. By comparing Figs. 7 and 8, it is noteworthy that the presence of Au increases the relative intensity of the 1460 and 1585 cm^{-1} bands (with respect to, e.g. the 1620 cm^{-1} band intensity) on some Au/M-Al_2O_3. The presence of Au enhances the relative intensity of these two bands on Cu-Al_2O_3, Ce-Al_2O_3, and Li-Al_2O_3. On the other hand, those bands on Fe-Al_2O_3 were only slightly promoted by Au and for Ti-Al_2O_3 no enhancement was found. Since Au significantly promotes the activity of M-Al_2O_3, it is suggested that Au enhances the SCO activity via increasing the surface concentration of the amide- and imide-like intermediates. The Au/Ti-Al_2O_3 showed almost no increase in this band intensity compared to Ti-Al_2O_3. This seems to be consistent with its low activity found in this study. On the other hand, Cu-Al_2O_3 is the only M-Al_2O_3 catalyst that showed significant SCO activity in this study, but imide-like adspecies are not present on this catalyst, as indicated by Fig. 7. The SCO over Cu-Al_2O_3 may occur via a different mechanism, most likely via a Cu surface redox (or Mars–van Krevelen) mechanism, as suggested earlier [7,24,34–36]. The higher SCO activity of Au/Cu-Al_2O_3 than

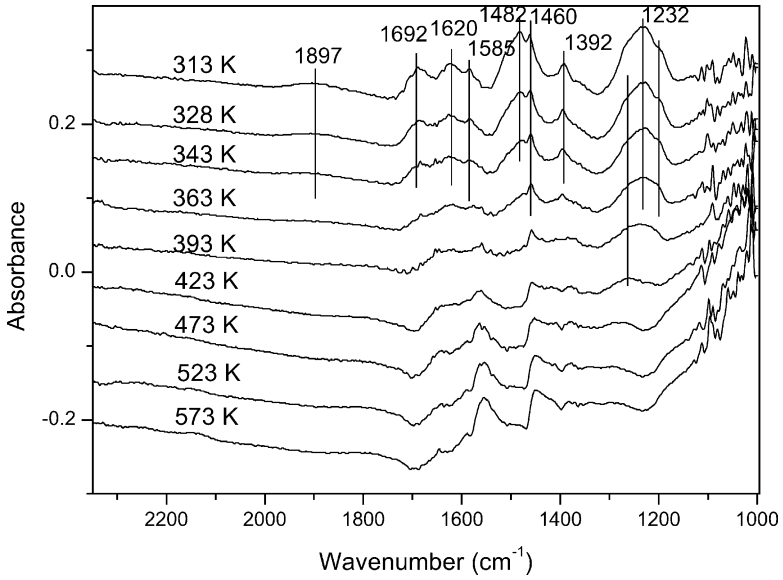

Fig. 9. FTIR spectra during a stepwise TPD of NH_3 on Au/Li-Al_2O_3.

Cu/Al_2O_3 observed in this study may indicate a synergistic effect of a gold-promoted NH_x intermediate and the reactivity of the CuO-phase.

The FTIR spectra of a stepwise TPD (sTPD) experiment of NH_3 adsorbed on Au/Li-Al_2O_3 are shown in Fig. 9. Similar experiments have been done for the other catalysts. However, only the results obtained for Au/Li-Al_2O_3 are shown because these spectra contain almost all the absorption features observed in this study. Upon heating first the NH_4^+ adspecies disappear, then subsequently the bands ascribed to surface –NH_2, the coordinated NH_3 on Lewis acid sites, and finally the 1460 cm^{-1} (imido) band. This desorption sequence seems to coincide with the expected adsorption strength of these adspecies. It is also interesting to note that the peak at 1460 cm^{-1} and a new peak at approximately 1560 cm^{-1} constitute the main IR absorption features above 473 K. The peak at around 1560 cm^{-1} is near the reported NO stretching band of nitroxyl species [25–30]. This implies that –NH adspecies may be converted to nitroxyl species at higher temperature. This suggests that an in situ SCR mechanism proposed earlier by Amblard et al. [13] may be involved for the gold-based catalysts. According to this mechanism surface NO_x may be formed and react with surface NH_x.

Readsorption of NH_3 at 313 K after this sTPD results in the same absorption bands as shown in Fig. 9, although the band intensities are a little bit smaller. This suggests that a sTPD experiment does not significantly alter the catalyst. A subsequent sTPO (sTPD under 2×10^3 Pa O_2, not shown here) does not generate any new absorption band on Au/Li-Al_2O_3 up to 423 K. However, the NH_3 adspecies seem to be more stable in the presence of 2×10^3 Pa O_2, as indicated by the prevalence of absorption bands to higher temperatures compared to the sTPD in Fig. 9. In addition, the 1460 cm^{-1} band in sTPO became more intense than that in sTPD. It should be mentioned that bands at 2192 and 2232 cm^{-1} were observed in the sTPO of Cu-Al_2O_3, Au/Al_2O_3, Au/Ti-Al_2O_3, Au/Fe-Al_2O_3, and Au/Cu-Al_2O_3 starting from 393 or 423 K in sTPO experiments. These two bands have been attributed to the N–N stretching mode of N_2^- adspecies [24–29]. However, the presence of this band did not warrant either a high SCO activity or a high selectivity to N_2 when compared to the reaction results of this study.

4. Discussion

In Table 3, the SCO activity of the Au/Cu-Al_2O_3 (Cu/Al = 1/10) catalyst is compared to literature data. It is somewhat difficult to rank the catalysts because the experimental conditions used were quite different. In addition, no systematic kinetic study of this SCO reaction has been reported, which makes a fair comparison of experimental data almost impossible. From Table 3, it can be concluded that an increase of NH_3 concentration (with a concurrent increase in NH_3 space velocity) does reduce the conversion level over both Ag-Cu/Al_2O_3 [18] and Pt/ZSM5 [8]. Pt/ZSM5 obviously showed a much more significant conversion loss. From kinetics a proportionally reduced conversion is expected upon increasing space velocity. Thus, the increased NH_3 partial pressure may only have a slight effect on the conversion. This suggests a low, maybe close to zero reaction order of NH_3 in this SCO reaction. That the IR absorption bands of NH_3 did not seem to be affected by the presence of oxygen supports the low NH_3 dependency. This implies that NH_3 is more abundant than oxygen on the surface. As a consequence, it is very likely that the reaction rate will be more dependent on the oxygen concentration. With this in mind, the Au/Cu-Al_2O_3 catalyst used in this study appears to be the most active SCO catalyst with an excellent N_2 selectivity.

Table 3
Ammonia oxidation over supported catalysts[a]

Catalyst	NH_3 (%)	O_2 (%)	SV_{NH_3}	T (°C)	X_{NH_3} (%)	S_{N_2} (%)	Reference	Remarks
5%Au/Cu-Al_2O_3 (573 K red.)	2	2	4	250	88	95	This study	
				300	100	95		
8.7%Cu-Al_2O_3 (573 K red.)	2	2	4	250	25	97	This study	
				300	72	98		
0.6%Pt/Fe-ZSM5 (773 K calc.)	0.1	2	5	200	45	99	[9]	H_2O and SO_2 slightly decreased activity
				250	99	92		
				300	99	90		
2.4%Fe-ZSM5 (773 K calc.)	0.1	2	5	350	78	92	[13]	
1.6%Fe-ZSM5 (773 K calc.)	0.1	2	5	350	63	92	[12]	Empty cell showed conversion
4.4%Cu-ZSM5	0.1	2	5	350	48	95	[12]	
1%Fe_2O_3-TiO_2 (773 K calc.)	0.1	2	2.5	300	37	91	[7]	Sulfate in Fe precursor improved performance
				350	83	78		
10%Cu/Al_2O_3 (773 K calc.)	1.14	8.21	4.3	250	12	97	[16]	
				300	90	96		
7.5%Ag-2.5%Cu/Al_2O_3 (773 K calc.)	1.14	8.21	4.3	250	92	99	[16]	
7.5%Ag-2.5%Cu/Al_2O_3 (773 K calc.)	0.1	10	0.5	200	92	92	[16]	
				250	100	92		
10%Ag/Al_2O_3 (473 K red.)	0.1	10	0.5	140	95	82	[15]	Calcined catalyst or that reduced at higher T was less active
				200	100	82		
8.4%Cu/Y (673 K calc.)	1.14	8.21	4.3	250	68	97	[6,14]	NaOH treatment increased activity
				300	100	98		
4.1%Pd/ZSM5 (773 K calc.)	0.1	4	1	200	46	89	[8]	Reduced Pd catalyst showed higher low-T activity
				250	94	75		
				300	98	81		
2.5%Pt/ZSM5 (773 K calc.)	0.1	4	1	200	99	71	[8]	H_2O decreased activity but increased selectivity
				250	100	41		
2.5%Pt/ZSM5 (773 K calc.)	4	4	40	250	77	63	[8]	
				300	95	50		

[a] The NH_3 space velocity, SV_{NH_3}, has a unit of ml NH_3/(min g) catalyst.

Gang et al. [17] observed a large effect of pretreatment for Ag/Al_2O_3. Prereduction at 473 K resulted in a higher activity for SCO reaction than a pretreatment of reduction or calcination at 773 K. Fig. 3 also indicates a strong effect of the pretreatment on the performance of Cu-Al_2O_3. It implies that oxidic Cu is more active for SCO than reduced Cu. Pradier et al. [36] reported that surface oxygen on Cu(1 1 0) favors abstraction of hydrogen from NH_3. This suggests that the step of hydrogen abstraction from NH_3 by surface oxygen leads to subsequent conversion of NH_3. This kind of mechanism has been discussed earlier: surface oxygen abstracts hydrogen from NH_3 to form surface hydroxyl and amide, as well as subsequent imide and adsorbed N. However, the reaction mechanism may be quite different for a reduced metallic surface and an oxidic surface [34–36]. It should be noted that the test conditions used in this study seem to keep the surface more reduced. This can be derived from the observation in Fig. 3 that the activity in the second heating cycle of the calcined Cu-Al_2O_3 was almost the same as that of the reduced one.

Another factor that may affect the SCO activity is the surface acidity. It is expected that an acidic surface should enhance NH_3 adsorption. However, such an enhanced adsorption could have a negative effect on SCO because surface NH_3 may be the more abundant species as discussed earlier. This is supported by the observation that a post treatment with NaOH increases the SCO activity of several catalysts [8,16]. On the other hand, Long and Yang [9] attributed the observed performance of Fe-TiO_2 prepared from sulfate-precursor in SCO to the effect of surface sulfate. However, this sulfate-containing Fe-TiO_2 actually showed a lower NH_3 conversion but a somewhat higher N_2 selectivity, similar to the effect of the inclusion of SO_2 in

the feed [7,9]. Therefore, a less acidic surface may favor a high activity in SCO.

Ammonia adsorption is used frequently to characterize the surface acidity. Davydov [22] commented from the work of Svatos et al. [37] that the asymmetric deformation vibration of ammonia molecules is sensitive to the nature of the cation. This comment was cited in later publications, e.g. [22,24–30] where more than one type of Lewis acid sites were used to explain the IR spectra in the range of 1100–1300 cm^{-1}. Svatos et al. [37] examined the IR spectra of many solid metal amine complexes. If their data of asymmetric bending band frequency are re-plotted versus the symmetric deformation band frequency, it appears that most of the data fall within a window of 1590–1630 and 1250–1320 cm^{-1}. This suggests that the NH_3 deformation band may not be very sensitive to the cation characteristics. This suggestion is consistent with the conclusions of Svatos et al. [37] who reported that the rocking band frequency is most sensitive to the nature of the N–M bond. Davydov [22] also showed that the symmetric deformation band of NH_3 on Cl-Al_2O_3, Al_2O_3, and Na^+-Al_2O_3 is at 1260, 1240, and 1230 cm^{-1}, respectively. This suggests that the strength of Lewis acid site may only cause a limited band shift. This makes the attribution of the broad band around 1200–1300 cm^{-1} in Figs. 7–9 to multi-Lewis acid sites ambiguous. The shoulder band at around 1190 cm^{-1} shown in Figs. 7–9 could also be attributed to molecularly adsorbed NH_3 on the reduced metal, since a 1180 cm^{-1} band has been reported on Cu(1 1 0) [36] and a 1190 cm^{-1} band on reduced Fe_2O_3 [22]. However, the intensity of the 1190 cm^{-1} band did not decrease in the presence of 2×10^3 Pa of oxygen, whereas a quick decrease of the intensity upon O_2 admission was observed on Cu(1 1 0) [36]. This again indicates that NH_3 is more abundant on the surface. From the trend of concurrent band disappearance during sTPD and sTPO, the shoulder band around 1190 cm^{-1} can be attributed to the rocking mode of $–NH_2$ associated with surface amide or hydrazine. Adsorbed amide and hydrazine species can only be distinguished by the $\nu_{N–N}$ mode of hydrazine. However, on TiO_2 and TiO_2-supported CrO_x, CoO_x, Fe_2O_3, and CuO [24,25,28,29], this mode was assigned to a band at 1210–1225 cm^{-1}, which is close to the region of the symmetric deformation mode of NH_3 coordinated on Lewis acid sites. Amblard et al. [13] also questioned the possibility of surface hydrazine based on the tendency of hydrazine decomposition into NH_3. Actually, it has been reported that both NH_3 and N_2H_4 adsorption result in very similar IR spectra on calcined Ni/Al_2O_3 [13] and TiO_2-supported oxides [24,25,28]. This makes a definite assignment of surface hydrazine almost impossible. Nevertheless, IR studies can clearly identify the presence of $–NH_2$ surface species by its less controversial rocking and asymmetric deformation modes around 1160–1190 and 1550–1580 cm^{-1}, respectively.

The presence of surface $–NH_2$ indicates the dissociative adsorption of NH_3 and/or the presence of H-abstraction on the surface. Its subsequent dissociation to imide adspecies can be identified by the IR band of δ(NH) at 1410–1460 cm^{-1}. Such a sequential NH_3 dissociation (hydrogen abstraction) is considered to be the mechanistic route to N_2, NO, and N_2O formation in SCO reaction [13,22,24,32]. Ramis et al. [24] proposed the formation of hydrazine as a critical step toward N_2 formation, whereas a surface imide is apt for NO formation via nitroxyl species. Amblard et al. [13] questioned this hydrazine-involved mechanism and favor an in situ SCR mechanism in which the surface NO_x can be reduced by NH_3. The further activation of surface NH_x is considered as a possible rate-limiting step in the mechanism of SCR. In this study, we observed that

(a) Au significantly enhances the SCO activity of M-Al_2O_3; and
(b) the IR band of surface imide-species is increased by the addition of Au.

The presence of Au seems to enhance H-abstraction of NH_3. The enhanced concentration of imide and the higher SCO activity is consistent with the limiting step of the mechanism of SCR discussed above. However, the IR analysis in this study could not identify the mechanistic route to N_2, and NO_x selectivity. From the observation that the SCO selectivity of Au catalysts strongly depends on the type of MO_x additive, it seems that the SCO selectivity is determined by certain metal–support interaction. Our results show that the selectivity toward N_2, N_2O or NO can be steered into the desired direction by a proper choice of the additive.

5. Conclusions

1. Cu-Al_2O_3 was found to be an active catalyst and very selective to N_2 consistent with literature data. Al_2O_3, TiO_2, Ti-Al_2O_3, Fe_2O_3, Fe-Al_2O_3, Li-Al_2O_3, Ce-Al_2O_3, and Li–Ce-Al_2O_3 are inactive for SCO at temperatures below 673 K.
2. The addition of Au to the above-mentioned M-Al_2O_3 results in a significant enhancement of the SCO activity. However, the activity and selectivity are very dependent on the M-Al_2O_3 used. Au/Cu-Al_2O_3 and Au/Li–Ce-Al_2O_3 are the two most active catalysts used in this study, where a 50% NH_3 conversion can be achieved at approximately 484 and 516 K, respectively. However, the Au/Cu-Al_2O_3 shows a N_2 selectivity above 90%, whereas the Au/Li–Ce-Al_2O_3 has a maximum N_2 selectivity of only 60% at 523 K. The selectivity of this catalyst to N_2O formation increases with increasing temperature and reaches 80% at the maximum temperature used in this study viz. 673 K. This catalyst may be a promising catalyst for the production of N_2O. This suggests that Au promotes the SCO activity and that the selectivity to N_2, N_2O or NO can be steered into the desired product by a proper choice of the oxidic additive.
3. FTIR analysis of adsorbed species was carried out on selected M-Al_2O_3 and Au/M-Al_2O_3 catalysts. The

adspecies identified includes NH_4^+ on Brønsted acid sites, NH_3 on Lewis acid sites, amide (or hydrazine), and imide. The assignment to hydrazine could be controversial because some of its absorption bands fall in the range of NH_3 absorption. It was found that the addition of Au significantly enhances the intensity of an absorption band at 1460 cm^{-1}, which is tentatively assigned to surface imido-species. Therefore, the enhanced SCO activity by the addition of Au is attributed to the increased surface concentration of this imido-species.

Acknowledgements

SDL would like to thank the Netherlands Organization for Scientific Research (NWO) and the National Science Council in Taiwan, ROC (NSC) for cosponsoring a summer research-visit to the Leiden Institute of Chemistry, under the Agreement for Scientific Cooperation between NWO and NSC.

References

[1] A.A. Ivanov, V.S. Chernyavsky, M.J. Gross, A.S. Kharitonov, A.K. Uriarte, G.I. Panov, Appl. Catal. A 249 (2003) 327.
[2] H. Orita, H. Kondoh, H. Nozoye, J. Catal. 177 (1998) 217.
[3] Kirk-Othmer Encyclopedia of Chemical Technology, vol. 15, Wiley, 1981, p. 856.
[4] N.I. Il'chenko, G.I. Golodet, J. Catal. 39 (1975) 57.
[5] F. Cavani, F. Trifiro, Catal. Today 4 (1989) 253.
[6] A. Wollner, F. Lange, Appl. Catal. A 94 (1993) 181.
[7] T. Curtin, F.O. Regan, C. Deconinck, N. Knuttle, B.K. Hodnett, Catal. Today 55 (2000) 189.
[8] L. Gang, B.G. Anderson, J. van Grondelle, R.A. van Santen, Catal. Today 61 (2000) 179.
[9] R.Q. Long, R.T. Yang, J. Catal. 207 (2002) 158.
[10] Y. Li, J.N. Armor, Appl. Catal. B 13 (1997) 131.
[11] R.Q. Long, R.T. Yang, Catal. Lett. 78 (2002) 353.
[12] M. Amblard, R. Burch, B.W.L. Southward, Appl. Catal. B 22 (1999) L159.
[13] M. Amblard, R. Burch, B.W.L. Southward, Catal. Today 59 (2000) 365.
[14] R.Q. Long, R.T. Yang, Chem. Commun. 1651 (2000).
[15] R.Q. Long, R.T. Yang, J. Catal. 201 (2001) 145.
[16] L. Gang, J. van Grondelle, B.G. Anderson, R.A. van Santen, J. Catal. 186 (1999) 100.
[17] L. Gang, B.G. Anderson, J. van Grondelle, R.A. van Santen, Appl. Catal. B 40 (2003) 101.
[18] L. Gang, B.G. Anderson, J. van Grondelle, R.A. van Santen, W.J.H. van Gennip, J.W. Niemanstverdriet, P.J. Kooyman, A. Knoester, H.H. Brongersma, J. Catal. 206 (2002) 60.
[19] M. Haruta, N. Yamada, T. Kobayashi, S. Iijima, J. Catal. 115 (1989) 301.
[20] G.C. Bond, D.T. Thompson, Catal. Rev.-Sci. Eng. 319 (1999) 41.
[21] A.C. Gluhoi, M.A.P. Dekkers, B.E. Nieuwenhuys, J. Catal. 219 (2003) 197.
[22] A.A. Davydov, in: Infrared Spectroscopy of Adsorbed Species on the Surface of Transition Metal Oxides, Wiley, 1990.
[23] G. Busca, J. Mol. Catal. 43 (1987) 225.
[24] G. Ramis, L. Yi, G. Busca, M. Turco, E. Kotur, R.J. Willey, J. Catal. 157 (1995) 523.
[25] M.A. Larrubia, G. Ramis, G. Busca, Appl. Catal. B 30 (2001) 101.
[26] G. Ramis, M.A. Larrubia, G. Busca, Top. Catal. 11/12 (2000) 161.
[27] G. Ramis, L. Yi, G. Busca, Catal. Today 28 (1996) 373.
[28] J.M.G. Amores, V.S. Escribano, G. Ramis, G. Busca, Appl. Catal. B 13 (1997) 45.
[29] G. Bagnasco, G. Peluso, G. Russo, M. Turco, Busca, G. Ramis, G., in: R.K. Grasselli, et al. (Eds.), 3rd World Congress on Oxidation Catalysis, Elsevier, Stud. Surf. Sci. Catal. 110 (1997) 643.
[30] H. Zou, J. Shen, Thermochim. Acta 351 (2000) 165.
[31] J.B. Peri, J. Phys. Chem. 69 (1965) 231.
[32] S. Kagami, T. Onishi, K. Tamatu, J. Chem. Soc. Faraday Trans. I 80 (1984) 29.
[33] A.A. Tsyganenko, D.V. Pozdnyakov, V.N. Filimonov, J. Mol. Struct. 29 (1975) 299.
[34] X.-C. Guo, R.J. Madix, Surf. Sci. 367 (1996) L95.
[35] R.W. Mayer, M. Havecker, A. Knop-Gericke, R. Schlogl, Catal. Lett. 74 (2001) 115.
[36] C.-M. Pradier, A. Adamski, C. Methivier, I. Louis-Rose, J. Mol. Catal. A 186 (2002) 193.
[37] G.F. Svatos, D.M. Sweeny, S.-I. Mizushima, C. Curran, J.V. Quagliano, J. Am. Chem. Soc. 79 (1957) 3313.